

Physics

Physics Research Publications

Purdue University

Year 2010

Acoustic and electrical property changes
due to microbial growth and biofilm
formation in porous media

C. A. Davis L. J. Pyrak-Nolte E. A. Atekwana

D. D. Werkema M. E. Haugen



Acoustic and electrical property changes due to microbial growth and biofilm formation in porous media

Caroline A. Davis,¹ Laura J. Pyrak-Nolte,² Estella A. Atekwana,³ Douglas D. Werkema Jr.,⁴ and Marisa E. Haugen²

Received 31 August 2009; revised 31 January 2010; accepted 19 February 2010; published 16 July 2010.

[1] A laboratory study was conducted to investigate the effect of microbial growth and biofilm formation on compressional waves, and complex conductivity during stimulated microbial growth. Over the 29 day duration of the experiment, compressional wave amplitudes and arrival times for the control (nonbiostimulated) sample were observed to be relatively uniform over the scanned 2-D region. However, the biostimulated sample exhibited a high degree of spatial variability in both the amplitude and arrival times, with portions of the sample exhibiting increased attenuation (~80%) concurrent with an increase in the arrival times, while other portions exhibited decreased attenuation (~45%) and decreased arrival times. The acoustic amplitude and arrival times changed significantly in the biostimulated column between days 5 and 7 of the experiment, consistent with a peak in the imaginary conductivity (σ'') values. The σ'' response is interpreted as recording the different stages of biofilm development with peak σ'' representing maximum biofilm thickness and decreasing σ'' representing cell death or detachment. Environmental scanning electron microscope imaging confirmed microbial cell attachment to sand surfaces and showed apparent differences in the morphology of attached biomass between regions of increased and decreased attenuation. The heterogeneity in the elastic properties arises from the differences in the morphology and structure of attached biofilms. These results suggest that combining acoustic imaging and complex conductivity techniques can provide a powerful tool for assessing microbial growth or biofilm formation and the associated changes in porous media, such as those that occur during bioremediation and microbial enhanced oil recovery.

Citation: Davis, C. A., L. J. Pyrak-Nolte, E. A. Atekwana, D. D. Werkema Jr., and M. E. Haugen (2010), Acoustic and electrical property changes due to microbial growth and biofilm formation in porous media, *J. Geophys. Res.*, 115, G00G06, doi:10.1029/2009JG001143.

1. Introduction

[2] Microorganisms have the ability to create micro-environments and niches in subsurface sediment environments by forming biofilms. Biofilms are created by the attachment, growth, and proliferation of microorganisms at mineral grain surfaces. These highly organized microbial systems consist of microbial cells, microbial byproducts, nutrients, substrates, and solid surfaces [Cunningham *et al.*, 1991; Marshall, 1992]. An important aspect of microbial attachment and growth on mineral surfaces is the production of a “pseudoglue” material consisting of exopolymeric substances (EPS), which helps to bind the microbes to surfaces.

The EPS that connects microbes to mineral particles is a key factor in clogging of sediment pore spaces and fluid flow pathways [Baveye *et al.*, 1998]. Studies have shown that biofilm development significantly reduces the porosity (by 50–90%) and permeability (by 95–99%) of porous media [e.g., Bouwer *et al.*, 2000; Dunsmore *et al.*, 2004]. Hence, microbial colonization of mineral surfaces and the proliferation of biofilms can have a profound effect on the physico-chemical properties of subsurface environments, influencing fluid flow and transport properties [e.g., Cunningham *et al.*, 1991; Baveye *et al.*, 1998; Brovelli *et al.*, 2009].

[3] Such microbial transformations of subsurface media are often coupled; occurring over a wide range of spatial and temporal scales, thus making it difficult to assess the extent of these dynamic microbial induced alterations. In addition, while biofilms are more readily studied in bioreactors, flasks, tanks, etc., they are more difficult to study in porous media [e.g., Cunningham *et al.*, 1991]. For example, the thickness and morphology of biofilms can be quantified using a variety of microscopy techniques such as confocal scanning laser or atomic force microscopy [e.g., Ahimou *et al.*, 2007; Yerly *et al.*, 2008]. Unfortunately, due to the surface roughness of

¹Department of Geological Sciences and Engineering, Missouri University of Science and Technology, Rolla, Missouri, USA.

²Department of Physics and Department of Earth and Atmospheric Sciences, Purdue University, West Lafayette, Indiana, USA.

³Boone Pickens School of Geology, Oklahoma State University, Stillwater, Oklahoma, USA.

⁴U.S. Environmental Protection Agency, Las Vegas, Nevada, USA.

sediment grains and the inherent difficulties of making such measurements when biofilms are found in geologic material, use of the above listed microscopy techniques is often limited. It is thus essential to develop techniques and proxy indicators that can provide spatiotemporal information on biofilm forming processes especially in field settings.

[4] Geophysical methodologies, such as seismic and electrical methods have the potential to provide a minimally invasive option to remotely detect, characterize and/or quantify the spatial distribution of biogeochemical processes [e.g., Williams *et al.*, 2005; Atekwana *et al.*, 2006; DeJong *et al.*, 2006; Atekwana and Slater, 2009; Slater *et al.*, 2009] and the induced changes in the physical properties of geologic media. The effects of biofilm formation on geophysical properties are currently not well understood, and require further study to determine how the mechanical properties of the geologic media are directly or indirectly affected by microbial activities.

[5] Understanding the mechanical properties of biofilms, such as attachment and detachment, is important for assessing biofilm processes and behavior, as well as for the control of biofilms in industrial and medical environments [Stoodley *et al.*, 1999; Ahimou *et al.*, 2007]. Rheological measurements have shown that biofilms exhibit linear viscoelastic behavior [Stoodley *et al.*, 1999; Klapper *et al.*, 2002; Ahimou *et al.*, 2007]. Acoustic and seismic measurements depend on the rheological properties of the porous medium and fluids that are contained in the pore spaces [Li *et al.*, 2001]. Thus, variations in the temporal viscoelastic properties of biofilms as they develop and evolve suggests that seismic geophysical techniques may be used to assess biofilm distribution and processes in field situations. Although several studies have investigated the rheological properties of biofilms in laboratory settings [e.g., Stoodley *et al.*, 1999], it is not known how such soft gelatinous material affects seismic wave propagation in porous media in the absence of mineral precipitation. Such an understanding is critical for assessing the utility of seismic geophysical techniques for imaging biofilm spatial distribution and the effects of bioclogging in porous media at field scales.

[6] Most biogeophysical investigations have focused on geoelectrical techniques (see, for example, reviews by Atekwana *et al.* [2006] and Atekwana and Slater [2009]) for the investigation of temporal microbial-induced phenomena. Recent studies have focused on the effect of biogenic gases or microbial mediated mineral precipitation on wave propagation in sands and sediments [e.g., Williams, 2002; Williams *et al.*, 2005; DeJong *et al.*, 2006, 2010]. The present study advances the work of Williams *et al.* [2005] and DeJong *et al.* [2006] by investigating the effect of biofilm formation on the spatiotemporal seismic properties of porous media using an acoustic two-dimensional scanning method [e.g., Li and Pyrak-Nolte, 1998; Pyrak-Nolte *et al.*, 1999] in the absence of enhanced precipitation. The primary objective of this research was to investigate the acoustic and electrical property changes due to microbial growth and biofilm formation in porous media. We observed that changes in the acoustic wave properties coincided with peaks in the imaginary component of complex conductivity. Based, in part, on our previous microbial growth study [Davis *et al.*, 2006] which showed that peaks in imaginary conductivity were coincident with peaks in microbial cell and biofilm attachment and

scanning electron microscope (SEM) images, we suggest that changes in the acoustic wave properties may be the direct result of the presence of biofilms. Hence we suggest that variations in biofilm structure and morphology in our samples caused heterogeneity in the elastic properties of the porous media, and thus variations in acoustic wave attenuation and velocity. Acoustic and electrical methods have the potential to (1) provide diagnostic semiquantitative data for testing and validation of bioclogging models and numerical simulations used for assessing microbial induced changes in flow and transport properties, and (2) be used for assessing spatial or temporal variations in biomass distribution in subsurface environments (i.e., microbial enhanced oil recovery (MEOR), and engineered biobarriers).

2. Materials and Methods

2.1. Experimental Column Setup

[7] Rectangular experimental columns were fabricated from 3.2 mm thick clear acrylic, and measured 102 mm by 51 mm by 254 mm (width \times depth \times height). Two sets of experimental columns were constructed: two columns for acoustic wave measurements (e.g., Figure 1a) and two columns for complex conductivity (electrical) measurements (e.g., Figure 1b). The electrical columns were constructed with two Ag-AgCl current injection electrode coils (160 mm apart), and two Ag-AgCl potential electrodes (90 mm apart), which were installed between the current electrodes (Figure 1b). In addition, a plastic divider was installed in the center of the electrical columns (Figures 1b and 1c), constructed from a 190 mm long section of 32 mm inner diameter (1 mm thick) polyvinyl chloride pipe cut lengthwise. Emplacement of the divider was deemed necessary to reduce noise in the electrical data, after calibration measurements using NaCl solutions of known fluid conductivity without the divider showed that the phase shift (ϕ) error exceeded 1 mrad at 10 Hz. This ϕ error is in excess of what has previously been reported by other studies using similar complex conductivity equipment (<0.5 mrad below 10 Hz) [e.g., Abdel Aal *et al.*, 2006], and well beyond the relative ϕ accuracy (~ 0.2 mrad below 100 Hz) reported for this instrumentation by Slater and Lesmes [2002]. After placing the divider in the electrical columns the ϕ error decreased to <0.5 mrad, which was deemed to be an acceptable level.

[8] All columns were initially prepared similarly. All columns were wet-packed with silica sand saturated with sterile 25% BH (Bushnell Haas; Becton Dickinson) nutrient broth, and manually agitated to release any trapped air bubbles. The coarse grain (0.6–1.18 mm) ASTM 20/30 silica sand (Ottawa, IL) consisted of 99.8% silicon dioxide, 0.020% iron oxide, 0.06% aluminum oxide, 0.01% titanium oxide, $<0.01\%$ calcium oxide, $<0.01\%$ magnesium oxide, $<0.01\%$ sodium oxide, $<0.01\%$ potassium oxide. The sands were washed with deionized water (DI), air-dried, and disinfected by autoclaving prior to being packed in the columns. Accessory equipment (e.g., tubing, valves) and columns were disinfected with a 70% ethanol solution before the experiment. Fresh, sterile BH broth was circulated through the sand-packed columns using a peristaltic pump, and baseline acoustic and electrical measurements were collected on all columns prior to commencing the column experimental treatments. Then the experiment began with the following experimental treat-

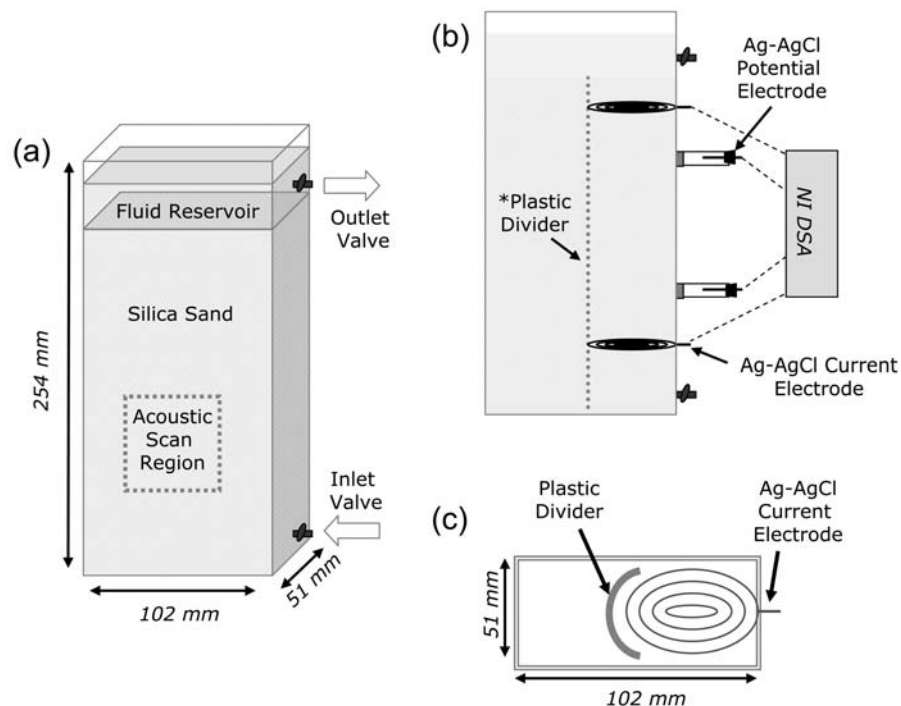


Figure 1. Schematic drawing showing the column setup for the (a) acoustic and (b and c) electrical columns. The 2-D acoustic scan region measures 60 mm \times 70 mm (width \times height). The drawing is not to scale.

ments. One set of columns (one electrical and one acoustic) was inoculated (herein called the biostimulated column) by saturating with 25% BH broth, 30 mM glucose, *Pseudomonas aeruginosa* PAO1 wild type bacteria culture, and 30 $\mu\text{g}/\text{mL}$ Gentamicin antibiotic. The *P. aeruginosa* bacteria strain (PAO1 Tn7-Gm-gfp) used in this experiment was obtained from the University of Denmark (Lyngby, Denmark) [e.g., Pamp and Tolker-Nielsen, 2007]. The PAO1 bacteria are a Gram-negative, rod-shaped, biofilm (slime) forming bacteria culture [e.g., Klausen *et al.*, 2003] commonly found in soil and water. The antibiotic was added to the biostimulated columns to inhibit growth of microorganisms besides that of the *P. aeruginosa*. The other set of columns had no bacteria inocula (herein called the control column), were saturated with 25% BH and 30 $\mu\text{g}/\text{mL}$ Gentamicin antibiotic and were used to collect background measurements. As this was a static experiment, the fluid in the columns remained stagnant during this experiment and the columns were not fed with additional nutrients.

2.2. Acoustic Wave Measurements

[9] An acoustic wave imaging system [e.g., Li and Pyrak-Nolte, 1998; Pyrak-Nolte *et al.*, 1999; Acosta-Colon *et al.*, 2009] was used to monitor the acoustic response of the experimental columns. The full-waveform imaging system consisted of two water-coupled plane wave transducers as source and receiver, computer-controlled linear actuators (Newport 850-B4 and Motion Master 2000), a high-voltage pulse generator (Panametrics PR1500), and an oscilloscope (Lecroy 9314L). Water-coupled transducers (12.7 mm diameter, 1 MHz central frequency) were used to ensure the same coupling between the transducers and the columns at all locations and over time. The columns were secured to a

platform placed in a tank of water and remained in place at laboratory conditions (22 $^{\circ}$ –24 $^{\circ}$ C) for the duration of the experiment. To perform an acoustic scan, the water-coupled transducers were positioned on opposite sides of the column (Figure 2) at a fixed distance from the column. The distance from the column was determined from the arrival time of the first reflection, i.e., the reflection from the water column interface. Over the 29 day duration of the experiments, the source and receiver path lengths were on average 29.69 mm and 29.37 mm, respectively, with a standard deviation of 680 microns. For the biostimulated column over the same time period, the source and receiver path lengths were on average 30.61 mm and 28.36 mm with standard deviations of 940 microns and 870 microns, respectively. After alignment of the source and receiver, full waveform measurements were recorded over a two-dimensional region of the column. Linear actuators were used to move the source and receiver in increments of 5 mm over the 60 mm by 70 mm acoustic scan region. An oscilloscope recorded and digitized the transmitted signals at each point in the scan region. Acoustic scans were collected over the 2-D scan region every 2–3 days for the 29 day experiment duration.

2.3. Complex Conductivity Measurement

[10] Complex conductivity (σ^*) measurements were collected at 40 frequency intervals between 0.1 and 1000 Hz using instrumentation based around a two-channel National Instruments (NI) dynamic signal analyzer [e.g., Slater and Lesmes, 2002]. Current (typically a swept sine wave) was injected through Ag-AgCl current electrode coils (Figure 1b) and the impedance magnitude ($|\sigma|$) and phase shift ϕ of the sample are recorded relative to a reference resistor [e.g., Slater and Lesmes, 2002]. The imaginary ($\sigma'' = |\sigma| \sin \phi$) part of the

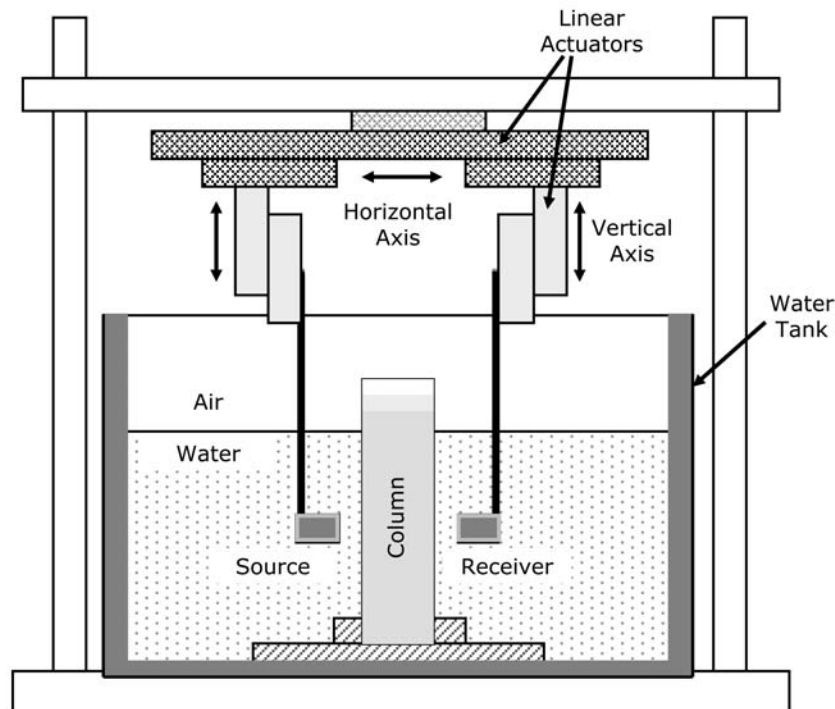


Figure 2. Drawing showing the acoustic imaging system setup and column placement in the water tank. The drawing is not to scale.

complex conductivity was then calculated from the measured $|\sigma|$ and φ , and the imaginary conductivity (σ'') is related to the polarization that occurs at interfaces [e.g., *Lesmes and Frye, 2001*]. Prior to introducing the experimental treatments and starting the experiments, the electrical measurement experimental uncertainty was determined from calibration measurements using NaCl solutions of known fluid conductivity (30–3000 $\mu\text{S}/\text{cm}$). The columns were then flushed with DI water prior to injection of the background and experimental solutions. Electrical measurements were collected 2–3 times per week for the 29 day duration of the experiment.

2.4. Geochemical and Sand Sampling

[11] Fluid temperature and pH were measured 1–2 times per week from fluid samples collected from the bottom valve of the columns. At the end of the experiment, the columns were destructively sampled by withdrawing fluid from the bottom valve and retrieving cores of sand. Cores of the wet sand were retrieved on a grid from different areas in the column based on the acoustic scan images. The sands were used for imaging with an environmental scanning electron microscope (ESEM) to investigate the sand surface characteristics and to confirm the presence of any biofilms. An FEI Quanta 600 ESEM operating at 25 kV, 14–89%, 5°–20°C, for accelerating voltage, relative humidity, and temperature, respectively, was used to image the sand grains.

3. Results

3.1. Acoustic Wave Measurement

[12] A full-waveform imaging system was used to monitor the effect of biofilm formation on transmitted compressional wave amplitude and arrival time. Figures 3 and 4 show a

20 microsecond window of compressional waves measured on the control and biostimulated samples from days 1, 5, and 29 of the experiment. The signals are chosen from two locations on the column referred to as position A and position E (see Figure 9 for the location on the column). For the two positions, the signals from the control column (Figure 3) did not change significantly in amplitude, arrival time or in phase over the duration of the experiment or between the two positions. However, the signals from the biostimulated column for the equivalent two locations differed in phase and amplitude and temporally over the duration of the experiment (Figure 4). On day 1, the signals from the biostimulated column at positions A and E are nearly identical (red curves in Figures 4a and 4b). On day 5, for both positions in the biostimulated column, the signal decreased in amplitude and a shift in phase is observed. By day 29, the compressional wave signal at position E in the biostimulated column (Figure 4b) had been strongly attenuated while the change in amplitude for position A (Figure 4a) depends on the phase, for example later arriving phases exhibit amplitudes slightly larger than those from day 1.

[13] Different methods can be used to quantify the change in amplitude of a signal, for example peak-to-peak amplitude of the first arrival or the maximum amplitude from a Fourier Spectrum. Because the signals in the biostimulated column exhibited phase shifts and amplitudes that vary with arrival time, we performed a time-frequency analysis, i.e., wavelet analysis to determine the amplitude and arrival time of the signals as a function of frequency. We used the Nolte-Hilbert wavelet transform [*Nolte et al., 2000*] that balances time-frequency localization without violating the wavelet admissibility condition that impedes the use of the Morlet wavelet transform.

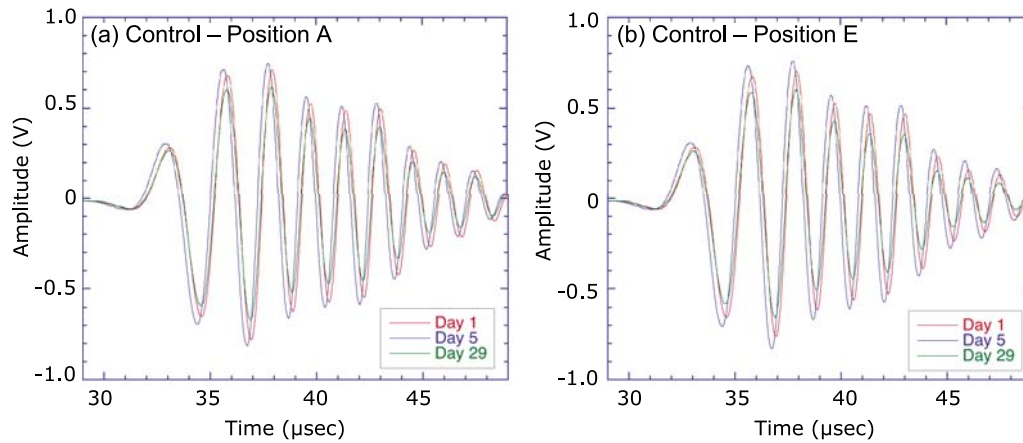


Figure 3. Transmitted compressional signals from the control column for days 1, 5, and 29 of the experiment for (a) position A and (b) position E. See Figure 9 for location of positions in the two-dimensional acoustic scans.

[14] Figures 5a and 5d show the wavelet transforms for the signals from the control column for days 1 and 29 of the experiment. The amplitude varies with frequency and between day 1 and day 29 the maximum amplitude decreased by 14%. For the biostimulated column position A (Figures 5b and 5e) from day 1 to day 29, the amplitude of the signal is observed to increase for several frequencies. However, a dramatic decrease in amplitude is observed for the signals collected at position E of the biostimulated column (Figures 5c and 5f). The maximum amplitude increased 7% for position A and decreased 80% for position B.

[15] The wavelet transforms also show that the transmitted compressional wave signals are dispersive, i.e., the arrival time varies as a function of frequency and, in particular, the low-frequency components of the signal arrive first. We extracted time-frequency dispersion curves from the wavelets by determining the arrival time of the maximum amplitude at each frequency. Figure 6a shows the time-frequency relationship for the control column for positions A and E for day 1 and day 29. The low-frequency components arrive first and the time dispersion is the same for both locations and over

time except for frequencies greater than 0.8 MHz. For the biostimulated column (Figure 6b), the time-dispersion relationship is the same at positions A and E. However, by the end of the experiment (day 29 in Figure 6b), the dispersion relationship is neither the same for the two positions nor the same as day 1 for the biostimulated column. For position A on day 29, the low-frequency components (<0.5 MHz) arrive later than those on day 1 but the high-frequency (>0.5 MHz) components arrive earlier (Figure 6b). The converse is observed for position E in the biostimulated column. The observed effect of biofilm development and microbial growth on arrival times and hence velocity is frequency dependent for the range of frequencies used in these laboratory experiments.

[16] From the data presented in Figures 4 and 6 for the biostimulated column, the acoustic response is observed to vary temporally and with frequency. To quantify the variations caused by biostimulation, we performed our analysis at a frequency of 0.5 MHz. For each scan, 168 signals were collected and a wavelet analysis was performed on each signal. From each wavelet, the maximum amplitude at a

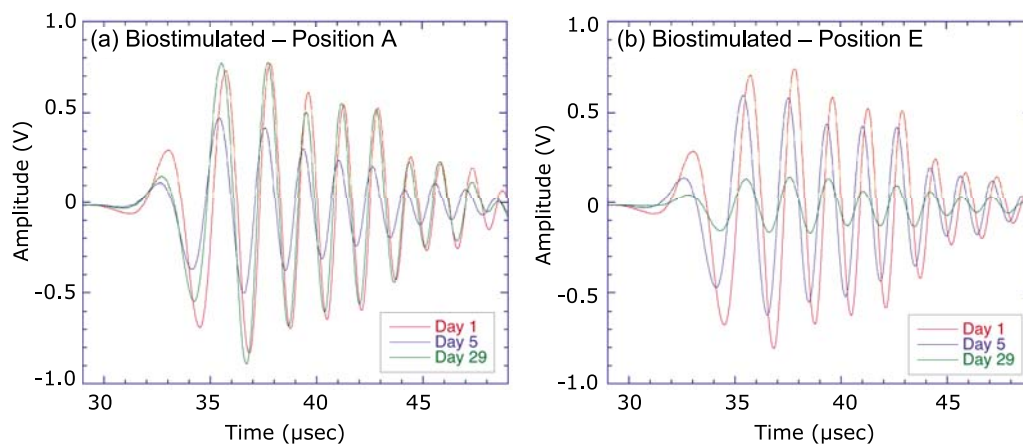


Figure 4. Transmitted compressional signals from the biostimulated column for days 1, 5, and 29 of the experiment for (a) position A and (b) position E. See Figure 9 for location of positions in the two-dimensional acoustic scans.

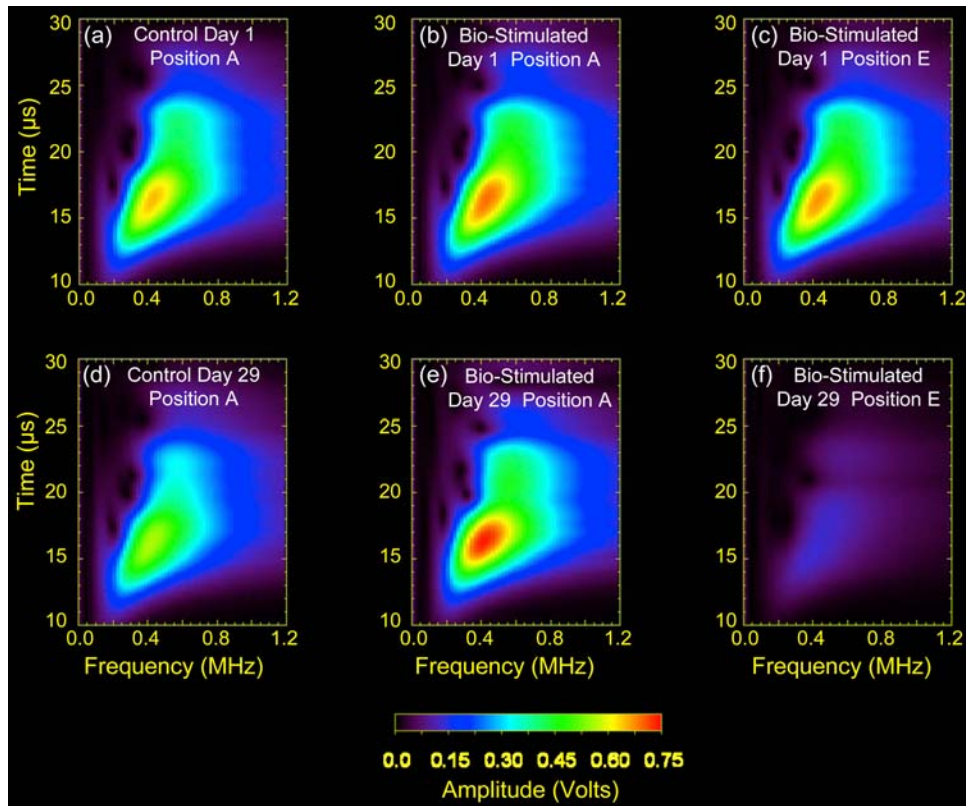


Figure 5. Wavelet transforms of the compressional wave signals from the (a and d) control column position A, (b and e) biostimulated column position A, and (c and f) biostimulated column position E for days 1 and 29 of the experiment.

frequency of 0.5 MHz was determined and the arrival time of the maximum amplitude was also recorded. These results were used to create two-dimensional acoustic maps of amplitude and arrival time (Figures 7 and 8).

[17] The time-progression 2-D acoustic maps of the transmitted acoustic amplitude and the group arrival time acquired from the control column are shown in Figures 7a and 7b, respectively. The baseline 2-D image from day 1 of the control column was relatively uniform in both the transmitted amplitude (Figure 7a) and time of arrival (Figure 7b) values,

except for the lower edges of the amplitude scan (Figure 7a) where slightly lower amplitudes were measured. Although the amplitude decreases slightly over the duration of the experiments, the measured amplitudes and arrival times became more spatially uniform over time.

[18] The time-progression 2-D acoustic maps of the transmitted amplitude and the group arrival time acquired from the biostimulated column are shown in Figures 8a and 8b, respectively. At the start of the experiment (day 1), the transmitted amplitude (Figure 8a) and time of arrival (Figure 8b)

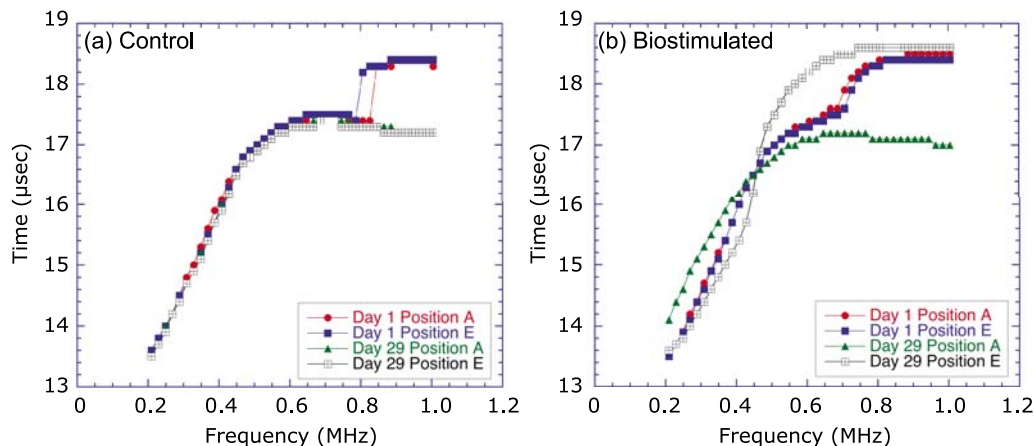


Figure 6. Time-frequency relationship extracted from the wavelet transforms for the (a) control column positions A and E for day 1 and day 29, and (b) biostimulated column positions A and E for day 1 and day 29.

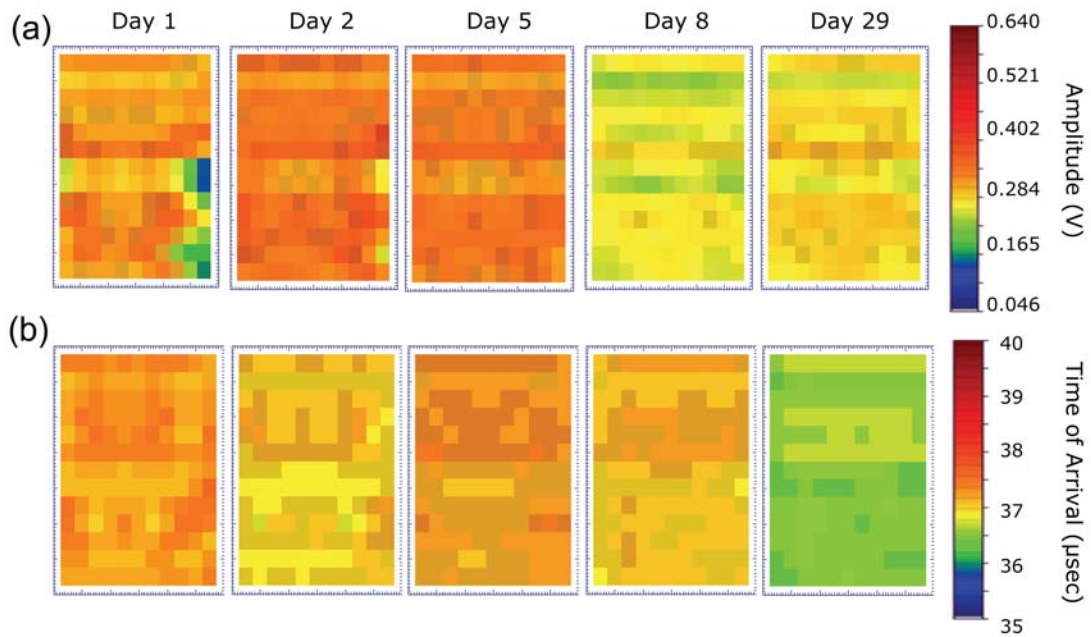


Figure 7. Two-dimensional map of the (a) compressional wave amplitude and (b) arrival time data for the control column for days 1, 2, 5, 8, and 29.

values are spatially relatively uniform over the scan region, as was observed in the time-frequency relationship (Figure 6b). By day 5, spatial variations are observed in the acoustic response over the scanned region in the biostimulated column, and a relatively consistent spatial trend in the amplitude response is noted on day 6 (image not shown), which persists through the end of the experiment. While a spatial trend is also observed in the arrival time response on day 6, the response is spatially variable through day 29

as compared to the control column (Figure 7b). The acoustic response measured on day 29 (Figure 8) exhibits both increases in amplitude and time of arrival in some regions, while other regions show a decrease. Overall, the compressional waves transmitted through the biostimulated column showed decreases in amplitude as large as ~80% and increases in arrival time on the order of ~3%.

[19] The temporal percent change in acoustic amplitude and arrival time relative to day 1 for both the biostimulated

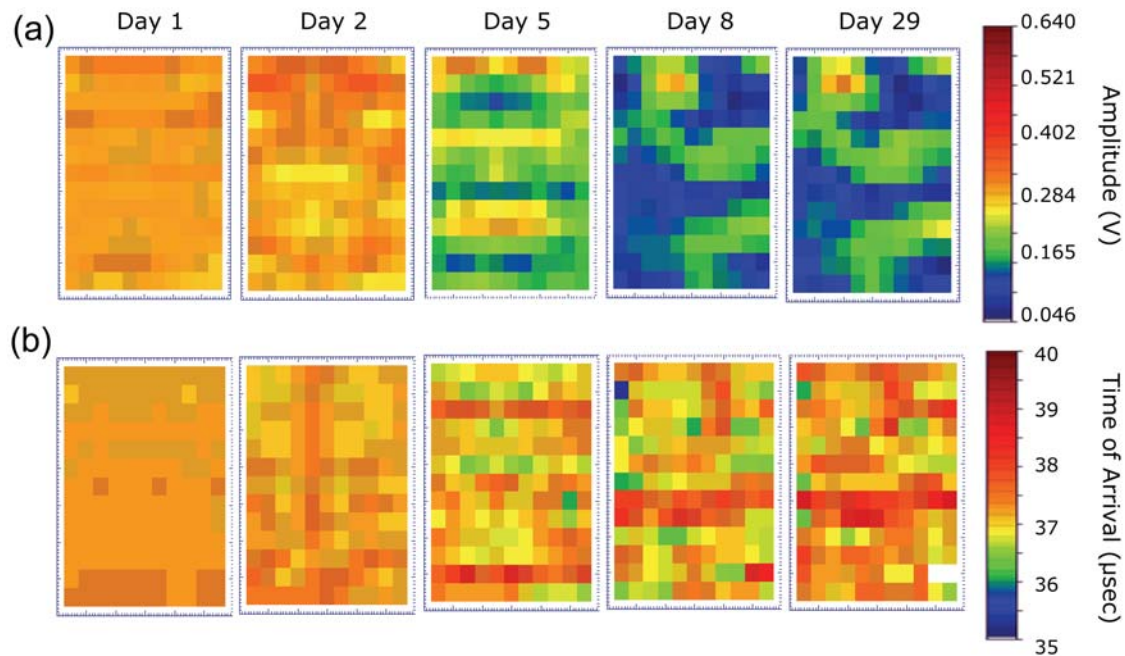


Figure 8. Two-dimensional map of the (a) compressional wave amplitude and (b) arrival time data for the biostimulated column for days 1, 2, 5, 8, and 29.

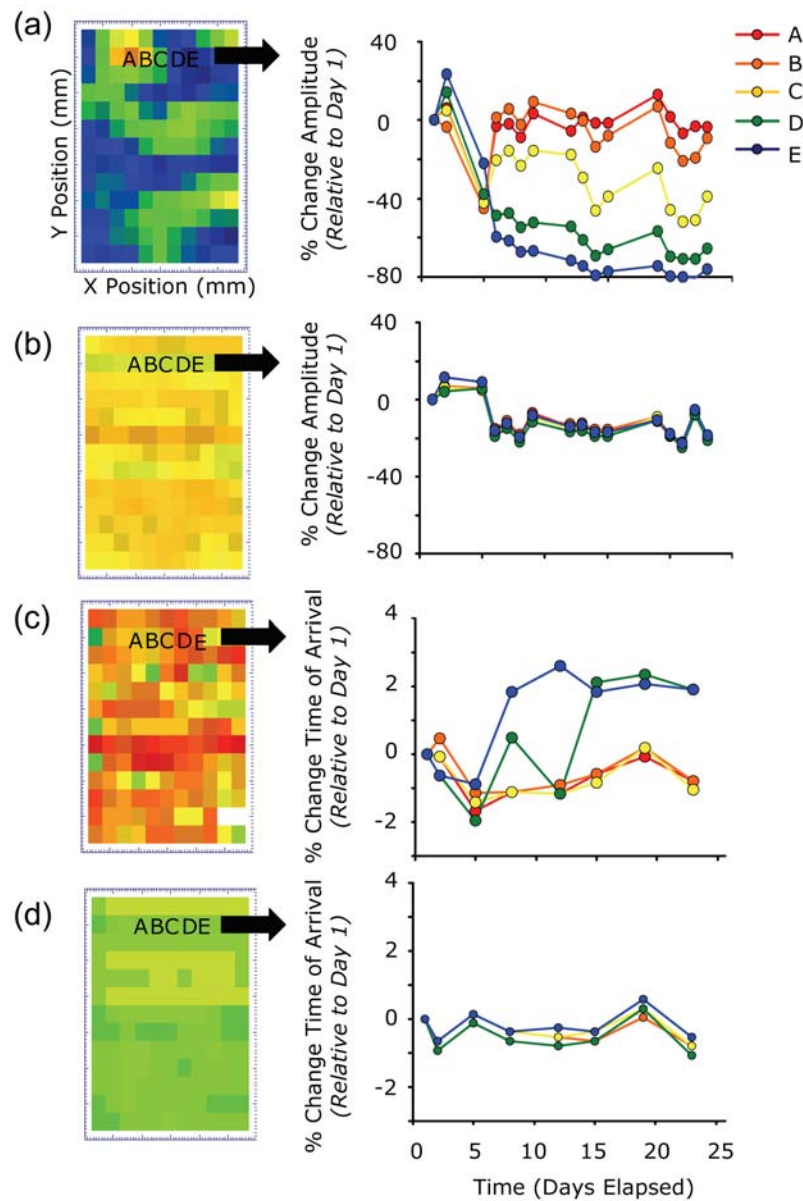


Figure 9. Two-dimensional amplitude scans obtained from day 29 for the (a) biostimulated and (b) control columns, with the select scan region (positions A–E) plotted temporally to the right. Similarly, the 2-D time of arrival scans obtained from day 29 for the (c) biostimulated and (d) control columns, with the select scan region (positions A–E) plotted to the right.

and control columns are shown in Figure 9. By day 5, the transmitted amplitude and arrival time measured on the biostimulated column (Figures 9a and 9c) deviate sharply from the baseline (day 1), whereas the acoustic response from the control column remains relatively steady compared to baseline (Figures 9b and 9d). Acoustic wave amplitudes observed from the biostimulated column are highly variable by day 6, both increasing and decreasing in amplitude in the selected region (Figure 9a; locations A–E). The arrival times for the biostimulated column (Figure 9c) by day 6 also vary in the selected region, though to a lesser degree. After day 6, the trend in amplitude and arrival times generally continued through the end of the experiment with the exception of one data location from the selected region. In contrast, the

amplitude and arrival time results from the control column remain relatively steady over time, and are consistent for all of the selected data points shown (Figures 9b and 9d; locations A–E) and do not exhibit the same heterogeneous behavior as observed for the biostimulated column (Figures 9a and 9c).

[20] We quantified the spatial variability in the control and biostimulated columns by examining the probability distribution of arrival times for each scan. The probability distribution from the control column narrowed over the duration of the experiment (Figure 10a) while the probability distribution from the biostimulated column broadened (Figure 10b). The average group arrival time (based on all measurement locations from a scan) does not change significantly (Figure 11a)

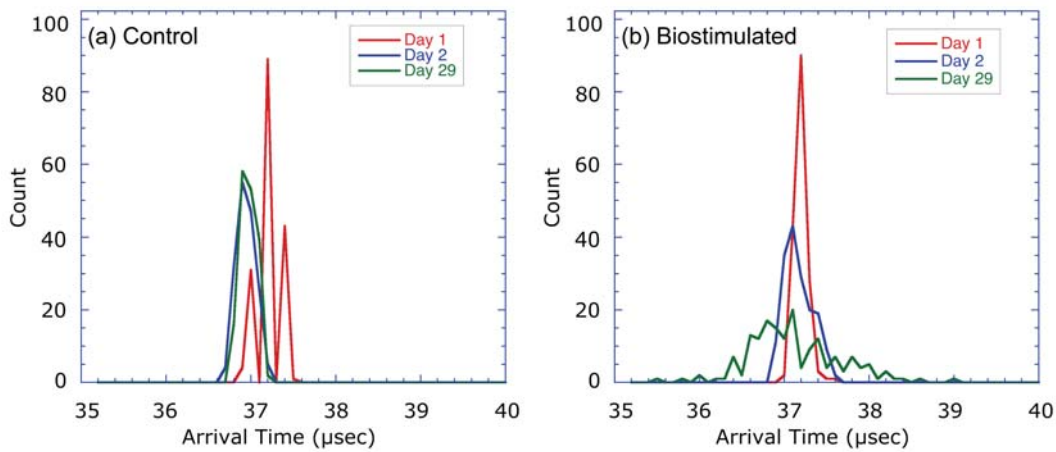


Figure 10. Histogram of the arrival time data for the (a) control and (b) biostimulated sample for days 1, 2, and 29.

for either column. However, the probability distribution (Figure 10b) gets broader with time for the biostimulated column. This is supported by the standard deviation of the probability distributions shown in Figure 11b. Over the duration of the experiment, the width of the probability distribution for the control column is relatively constant and narrow indicating a fairly homogenized distribution of acoustic properties (e.g., elastic moduli, porosity, etc.). On the other hand, the probability distribution for the biostimulated column broadens and the standard deviation increases with experimental time up until about 15 days. The acoustic properties of the biostimulated became more heterogeneous with time.

3.2. Complex Conductivity and Geochemical Measurement

[21] The results of the calibration tests conducted prior to the experiment indicate that experimental uncertainty associated with the ϕ measurements were generally less than 0.5 mrad at 10 Hz. The experimental σ'' results are reported at 10 Hz, as this is the frequency where the lowest phase shift error was observed during calibration measurements, and this

frequency is close to typical frequencies used in field electrical measurements.

[22] The results of the temporal σ'' and pH are shown in Figure 12. The σ'' measured from the biostimulated column (Figure 12a) increased by $\sim 220\%$ to peak values (2.29×10^{-5} S/m) on day 5 relative to preinjection (day -1) values (7.16×10^{-6} S/m), before steadily decreasing to near baseline values by day 14, and remained relatively consistent through day 23. The magnitude of the σ'' response measured from the control column was relatively small compared to the biostimulated column, varying by $\sim 1.09 \times 10^{-6}$ S/m over the duration of the experiment compared to 1.57×10^{-5} S/m for the biostimulated column. The pH values measured for the control column remained steady near a pH of 7 throughout the experiment (Figure 12b). The pH values measured from the biostimulated column, however, steadily decreased from a baseline pH value of 7 to near 4.4 on day 8, and remained steady at a pH of 4.4 to the end of the experiment.

3.3. Grain Surface Characteristics

[23] ESEM images obtained from destructive sampling of the biostimulated and control columns are shown in

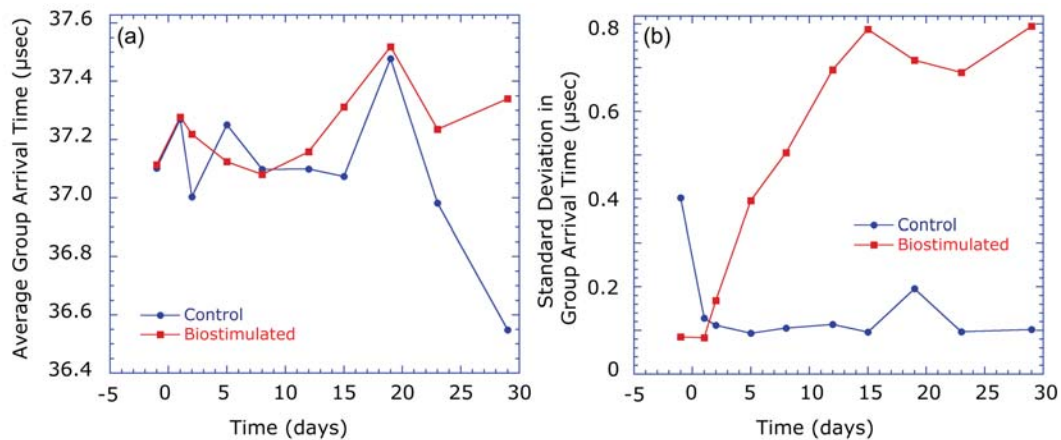


Figure 11. A comparison of the variation in (a) average arrival time and (b) standard deviation for the control and biostimulated samples as a function of experimental time.

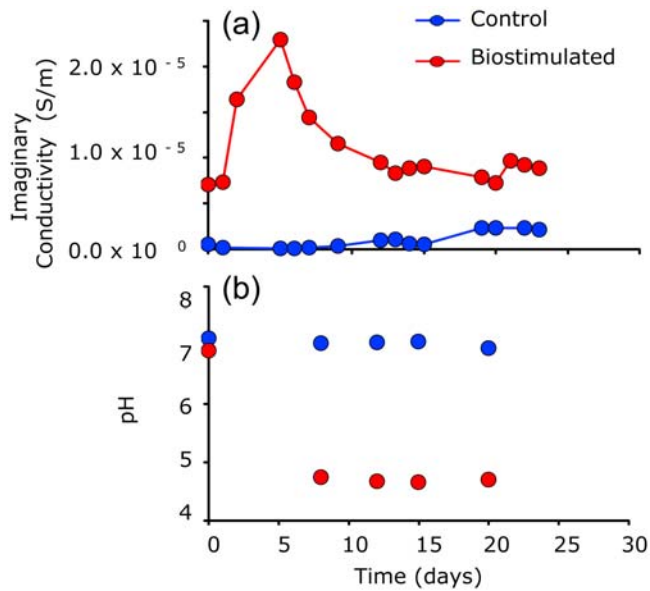


Figure 12. Plots showing the (a) temporal imaginary conductivity (at 10 Hz) and (b) pH results.

Figure 13. We observe differences in the biofilm structure between areas of increased and decreased amplitude in the biostimulated columns. ESEM images that are representative of the increased acoustic amplitude columns are shown in

Figures 13a and 13b. In these images, the surface texture is rough with a patchy covering of “biomaterial” or EPS covering portions of the sand grain. However, other portions of the grain are not covered and the surface of the grain is clearly visible. Although not clearly distinguishable in these images, rod-shaped bacterial cells are present in this biomaterial (Figures 13a and 13b). We note that during ESEM imaging of the increased amplitude sand samples, individual bacterial cells were not visible until the operating temperature of the ESEM was raised from 5° to 20°C, and the relative humidity was decreased from 89% to 14%, which effectively dried out the sample/biomaterial.

[24] ESEM images that are representative of the decreased acoustic amplitude samples from the biostimulated column are shown in Figures 13c and 13d. In contrast to the previous ESEM images (Figures 13a and 13b), the images obtained from the area of decreased acoustic amplitude (Figures 13c and 13d) indicate that a smooth biomaterial appears to completely cover the surface of the sand grain. Several holes and voids in the biomaterial covering the grain are also observed. Rod-shaped bacteria are also seen in these images on top of the biomaterial as well as along the inner sides of the void spaces. Upon viewing with the ESEM (at 5°C and 89%), the individual cells and attached biomass were clearly visible and appeared to remain the same even when the temperature was increased to 20°C (images not shown). No enhanced precipitation was observed on the ESEM images.

[25] The ESEM images of sand samples obtained from the control column (Figures 13e and 13f) were imaged with

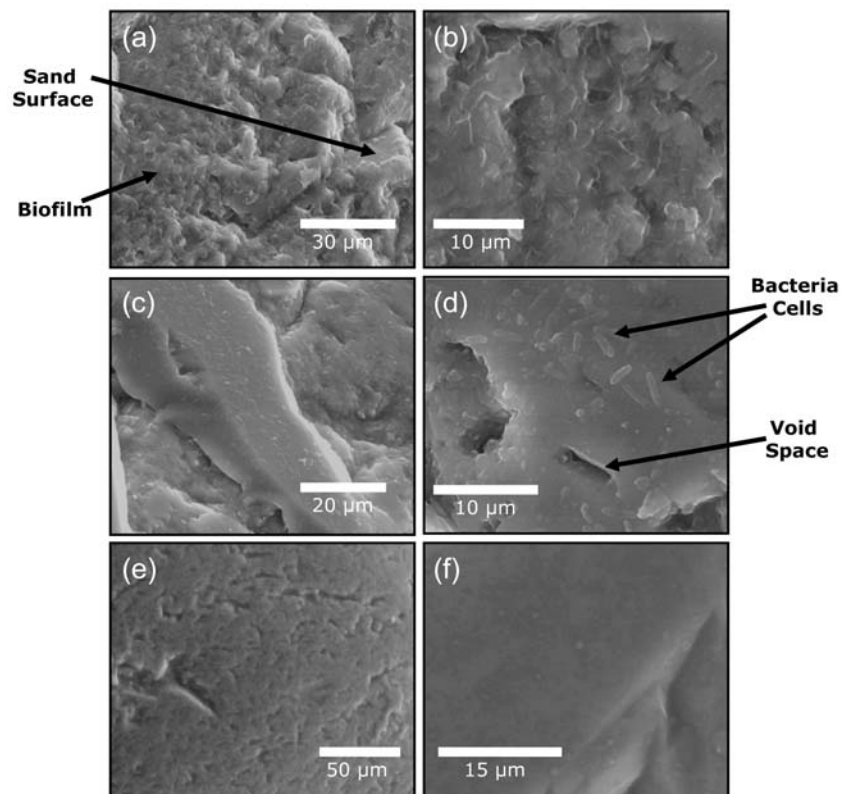


Figure 13. Environmental scanning electron microscope (ESEM) images from sand samples collected after column destruction. (a and b) Images from the biostimulated column collected from an area of increased amplitude on the 2-D acoustic scan, and (c and d) images from an area of decreased amplitude. (e and f) Images from the control column.

ESEM operating conditions of 25 kV, 89%, 5°C, for accelerating voltage, relative humidity, and temperature, respectively. No bacterial cells or biomass are apparent in these images. The surface of the silica sand grain is irregular but relatively smooth.

4. Discussion and Conclusions

4.1. Spatial Variability of Acoustic Properties

[26] Previous seismic studies have demonstrated that seismic methods are sensitive to the products of microbial activity in porous media, such as the production of biogenic gas [Williams, 2002] and enhanced biomineralization [Williams et al., 2005; DeJong et al., 2006]. Based on the fact that mineral precipitation was not induced or enhanced in our current experiment, and no large gas bubble formation was observed on the sides of the biostimulated columns (unlike that of Williams [2002]), we attribute the observed amplitude variation in the biostimulated sample in these experiments to biofilm development. This attribution is based on the observed microbes and biofilms in the ESEM images of samples at locations with enhanced/reduced acoustic attenuation.

[27] The results of our laboratory study indicate that biostimulation of a porous media alters the acoustic properties of the sediment both spatially and temporally. In physical models of sediments, wave propagation depends on the physical properties of the individual constituents (density, elastic moduli, etc., of both the fluid and solid components) of the granular medium and on the structural characteristics of the matrix. The major mechanisms of energy loss are scattering (when the wavelength of the signal approaches the size of the scatterer), frictional losses at grain-grain contacts, and viscous losses caused by relative motion between the pore fluid and the sediment frame. Bio-alteration can potentially alter the pore fluid properties (e.g., viscosity) as well as the mechanical properties of the sediment.

[28] The ESEM images confirm both the presence of bacteria and biomaterial in the biostimulated column, and confirm that the amount and structure (or texture) of the biomaterial varied at different locations in the sample (Figure 13). Furthermore, the ESEM images do not show mineral precipitation. The acoustic measurements taken at the locations of the ESEM images exhibited different trends in attenuation and group arrival times as observed in the acoustic maps and arrival time dispersion curves (Figures 6 and 8). From our data sets, an increase in the transmitted wave amplitude is observed to occur when grains had a patchy or nonuniform covering of biomaterial. A possible hypothesis is that small amounts of biomaterial enhance coupling between grains either at grain contacts or by coupling grains together. Nihei [1992] observed from numerical modeling and laboratory experiments that grain contacts were the primary sites of attenuation in dry and fluid-saturated granular media and can result in frequency-dependent attenuation coefficients caused by scattering at grain contacts. Work on granular media [Nihei, 1992; Liu and Nagel, 1992] has recognized that granular packings are complex structural systems composed of particles that have a finite number of contacts with neighboring particles and form a three-dimensional force-chain network. In such systems, small-amplitude vibrations are sensitive to the degree of contact

between particles. Thus, biofilm networks (hyphae) that link grains may alter the force-chain network of the sediment and potentially strengthen the contacts.

[29] Most locations in the biostimulated sand column exhibited a decrease in amplitude. ESEM images from these locations showed that the biomaterial coating the grains had a smooth texture and contained numerous void spaces/pores or channels (Figures 13c and 13d). Decreases in acoustic amplitude often result from biogenic gas production, weakening of grain contact/coupling, as well as dissipation caused by viscous losses as a bio-altered pore fluid moves relative to the frame, or by losses associated with the skeletal frame characterized by a complex moduli.

[30] The variability in the acoustic wave measurements presented here from the biostimulated column (e.g., Figures 8 and 9) suggests that more than one mechanism may be responsible for the variability in the spatiotemporal acoustic amplitude. Biofilm structures have been shown to be very heterogeneous, consisting of cell clusters, pores, channels, and EPS [Zhan et al., 2006]. It is also documented that thicker biofilms exhibit higher EPS yields, higher porosity, lower density, and higher water content [Zhan et al., 2006], whereas, thinner biofilms tend to have lower porosity, higher density, and lower water content. We infer from our results that spatial variations in acoustic amplitude and travel times most likely result from the nonuniform distribution of biomass and variations in the biofilm structure in porous media which affected the grain-to-grain coupling, pore geometry, fluid-solid coupling and elastic/viscoelastic response of the medium. Additional research is needed to determine the attenuation mechanism or competing mechanisms that result from biofilm evolution.

4.2. Temporal Variability of the Complex Conductivity

[31] In addition to the spatial variability in the acoustic wave amplitude, there is also significant temporal variation measured in the biostimulated column, as shown in the time-progression 2-D acoustic maps (Figure 8) and temporal plots (Figure 9a). Significant changes in the acoustic wave properties occurred in the biostimulated column between day 5 and day 7 of the experiment (Figure 8). These observed acoustic changes are consistent with a peak in the imaginary conductivity values on day 5 (Figure 12). In our earlier work [Davis et al., 2006], we demonstrated that imaginary conductivity measurements are uniquely sensitive to the physicochemical properties at grain-fluid interfaces, and showed that imaginary conductivity measurements may be used as a proxy indicator of microbial growth, attachment, and biofilm formation in porous media. In this earlier work, we observed peak increases in imaginary conductivity that generally paralleled peak increases in attached microbial cell concentrations and biofilms. While we did not measure the concentration of attached biomass or the thickness of biomass in the current experiment, our complex conductivity results are identical to the study by Davis et al. [2006]. Thus, we suggest that the peak changes observed in the imaginary conductivity response may reflect a peak in the concentration of attached biomass or biofilm thickness. Based on this assumption, we infer that the variations in the acoustic amplitude that occurred between days 5 and 7 are associated with the change in physical properties of the medium caused

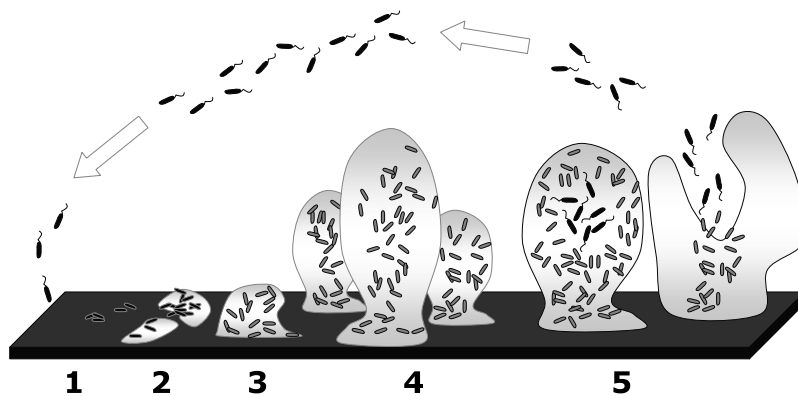


Figure 14. Drawing showing the different stages of biofilm development, including (1) reversible attachment of microbial cells, (2) irreversible attachment, (3) maturation and layering of biofilm, (4) maturation and maximum thickness, and (5) dispersion/detachment of microbial cells and biofilm (modified from <http://www2.binghamton.edu/biology/faculty/davies/research.htm-8/31/09>).

by peak microbial attachment and maximum biofilm thickness. We also note that there is a remarkable similarity in the temporal acoustic and electrical data presented here, and the relative time frame for biofilm development presented by *Davey et al.* [2003] as discussed below in section 4.3. This may be further evidence that biofilm development is a primary contributor to the observed geophysical response.

[32] Similar to *Davis et al.* [2006], we observed a consistent decrease in the imaginary conductivity after peak values were observed and for the remaining duration of the experiment. This decrease in the imaginary conductivity may be attributed to increased rates of detachment, dispersion, or cell death potentially due to nutrient limitations [*Davis et al.*, 2006; *Abdel Aal*, 2008]. A possible reason for the suggested increase in cell death or detachment may be the result of the accumulation of waste products (e.g., organic acids) and the low pH conditions that developed over time in the biostimulated column contributed to the death of the cells.

[33] Given the above discussion we suggest that the imaginary conductivity was responsive to the biofilm development (Figure 14). Initial attachment of cells to the surfaces (both reversible and irreversible) resulted in a small change in the imaginary conductivity (days 1–2, Figure 12). Studies by *Abdel Aal et al.* [2009] have suggested that attachment of cells to clean quartz sands (such as was used in this experiment) result in an enhancement of the imaginary conductivity of ~15%. Since we measured increases in the imaginary conductivity of >200%, we hypothesize that attachment, rapid colonization, and the production of biofilms may explain the peak in the imaginary conductivity values observed on day 5. Consequent death of cells resulting from possible accumulation of acids (evidenced by low pH) resulted in a rapid decrease in the imaginary conductivity as observed after day 5 (Figure 12). We also note that pH values remained constant after day 8 to the end of the experiment. In contrast to the imaginary conductivity, the acoustic wave amplitude after day 8 remained relatively constant through the end of the experiment (Figure 9). While dead cells have no electrical properties and hence the decrease in imaginary conductivity after day 5 [e.g., *Abdel Aal*, 2008], it is possible that a steady biofilm or EPS thickness remained in the pore geometries of

the porous media, hence no change was observed in the acoustic properties after day 8.

4.3. Effect of Biofilm Structure and Development on Acoustic Properties

[34] *Davey et al.* [2003] describes five different physiologies over the course of biofilm development by *P. aeruginosa*, including: (1) initial reversible attachment, (2) irreversible attachment, (3) maturation through layering of bacterial cell clusters, (4) maturation of cell clusters and maximum layer thickness, and (5) dispersion of bacteria cells from within the inner portion of the biofilm (Figure 14). In addition to the sequence of biofilm development described by *Davey et al.* [2003], the authors also provided a relative time frame for this development, where the third stage (or physiology) occurred at ~3 days of growth, the fourth stage after ~6 days of growth, and the fifth stage after ~9–12 days. *Klausen et al.* [2003] observed that the basic *P. aeruginosa* biofilm structure did not change appreciably after day 7, although the accumulation of biomass within the biofilm on day 7 had not yet reached a plateau. Therefore, the authors referred to the 7 day old biofilms as being mature biofilms. Further, *Davey et al.* [2003] stated that all stages of the sequential development may be present at the same time during the maturation of the biofilm. We note that no significant changes in the acoustic properties were observed in our columns after day 8.

[35] Physically, the presence of biofilms may alter grain contact coupling, decrease the volume and size of pores which alters the pore throat geometry, provide additional coupling among grains, or alter relative motion between the bio- alter pore fluid and the solid grains (i.e., viscous losses). All of the above will affect the sediment matrix stiffness and the elastic and/or visco-elastic moduli of the fluid-saturated media. In addition, if the microbial-induced alterations are not uniformly distributed throughout the sediment, then the sediment textural and mechanical properties may vary spatially leading to spatial heterogeneity in the seismic signatures (i.e., scattering).

[36] Wave scattering or interference from spatial heterogeneity of the medium is another mechanism that affects wave attenuation. In our experiments, air bubbles were not a

source of scattering because no gas formation was observed in the biostimulated sample. Scattering caused by a density contrast between the water-saturated sediment and the microbially altered sediment is not large and is therefore ruled out as a source of scattering. Thus, if scattering is the source of the observed spatial heterogeneity in the acoustic properties of the bio-stimulated sample, the cause of the scattering could be attributed to the spatial variation in elastic or viscoelastic moduli from microbial alteration of the grain contact, pore-filling material and/or biofilm connecting grains.

[37] Variations in pore geometries and elastic properties between regions of highly colonized, dense areas of biofilm (e.g., Figures 13c and 13d) and those with a patchy distribution of biomass (e.g., Figures 13a and 13b) may affect local permeability and pore pressure. When the porous media is excited by the passing acoustic wave, grain-scale heterogeneities (i.e., pore shape, saturation) will induce pressure gradients and cause pore fluid to be squeezed from compliant to less compliant regions. This movement of fluid results in viscous dissipation or “squirt-flow” mechanisms [e.g., Palmer and Traviolia, 1980; Mavko and Jizba, 1991]. Thus, we hypothesize that spatially nonuniform biofilm structure alters the pore geometry and elastic moduli which results in heterogeneous attenuation and travel times. The relatively high spatial variation observed in the acoustic data from our current study suggests that enhanced microbial growth has a variable as well as frequency-dependent effect on the elastic properties of porous media. The effect of the microbial growth on the elastic properties depends on the amount and stages of biofilm development. Future work should focus on delineating the competing attenuation mechanisms that arise from enhanced microbial growth and biofilms. In addition, further work is needed to quantify the relationship between the amount and type of biofilm present in a porous medium and the degree to which the acoustic signal is attenuated by the presence of biomass. Experiments that examine the effect of biofilm properties (such as thickness, density, porosity, viscosity, etc.) on seismic wave attenuation are needed.

[38] The geophysical results presented here are relevant to field applications that require information on the spatial distribution of subsurface biofilms. For example, microbial enhanced oil recovery activities use the in situ growth of microorganisms and biofilm formation to selectively plug highly permeable zones. However, up scaling our seismic laboratory measurements to the field scale will depend on spatial and temporal dispersion, as well as consideration of field site conditions, gas production, and precipitation effects, as quite probably these mechanisms are all involved in complex heterogeneous field settings. Furthermore, temporal dispersion connects frequency-dependent attenuation and velocity with elastic moduli, i.e., changes at grain contacts or pore filling. While, spatial dispersion connects wavelength with the size of the scatterer, that is, the size or spatial correlation length of microbially altered regions. Thus, increasing or decreasing seismic attenuation with frequency will provide information on the size of the altered region and on the spatiotemporal distribution of the biomass or bioclogging development. This potential surface mapping capability would yield new additional information on subsurface sites where microbial activity is of interest.

[39] **Acknowledgments.** This material is based in part on work supported by the National Science Foundation under grants OCE-0729642, EAR 0722410 (MRI), EAR 0525316, and REU award 0552918, and EPA Student Services contract EP07D000660. L.J.P.N. would like to acknowledge support from Geosciences Research Program, Office of Basic Energy Sciences, U.S. Department of Energy (DEFG02-97ER14785 08). S. Pamp and T. Tolker-Nielsen provided the *Pseudomonas* PAO1 Tn7-Gm-gfp strain to S. Rossbach, and we thank S. Rossbach for helpful discussions on growing the bacteria. Although this work was reviewed by EPA and approved for presentation, it may not necessarily reflect official Agency policy. Mention of trade names or commercial products does not constitute endorsement or recommendation by EPA for use.

References

- Abdel Aal, G. Z. (2008), Electrical properties of bacteria in sand columns: Live vs. dead cells, paper presented at Chapman Conference on Biogeophysics, AGU, Portland, Maine.
- Abdel Aal, G. Z., L. D. Slater, and E. A. Atekwana (2006), Induced-polarization measurements on unconsolidated sediments from a site of active hydrocarbon biodegradation, *Geophysics*, 71(2), H13–H24, doi:10.1190/1.2187760.
- Abdel Aal, G., E. Atekwana, S. Radzikowski, and S. Rossbach (2009), Effect of bacterial adsorption on low frequency electrical properties of clean quartz sands and iron-oxide coated sands, *Geophys. Res. Lett.*, 36, L04403, doi:10.1029/2008GL036196.
- Acosta-Colon, A., L. J. Pyrak-Nolte, and D. D. Nolte (2009), Laboratory-scale study of field of view and the seismic interpretation of fracture specific stiffness, *Geophys. Prospect.*, 57(2), 209–224, doi:10.1111/j.1365-2478.2008.00771.x.
- Ahimou, F., M. J. Semmens, P. J. Novak, and G. Haugstad (2007), Biofilm cohesiveness measurement using a novel atomic force microscopy methodology, *Appl. Environ. Microbiol.*, 73(9), 2897–2904, doi:10.1128/AEM.02388-06.
- Atekwana, E. A., and L. D. Slater (2009), Biogeophysics: A new frontier in Earth science research, *Rev. Geophys.*, 47, RG4004, doi:10.1029/2009RG000285.
- Atekwana, E. A., E. A. Atekwana, and D. D. Werkema (2006), Biogeophysics: The effects of microbial processes on geophysical properties of the shallow subsurface, in *Applied Hydrogeophysics*, NATO Sci. Ser., vol. 4, edited by H. Vereecken et al., pp. 161–193, Springer, New York.
- Baveye, P., P. Vandevivere, B. L. Hoyle, P. C. DeLeo, and D. Sanchez de Lozada (1998), Environmental impact and mechanisms of the biological clogging of saturated soils and aquifer materials, *Crit. Rev. Environ. Sci. Technol.*, 28(2), 123–191, doi:10.1080/10643389891254197.
- Bouwer, E. J., H. H. M. Rijnaarts, A. B. Cunningham, and R. Gerlach (2000), Biofilms in porous media, in *Biofilms II: Process Analysis and Applications*, edited by J. D. Bryers, pp. 123–158, Wiley-Liss, Wilmington, Del.
- Brovelli, A., F. Malaguerra, and D. A. Barry (2009), Bioclogging in porous media: Model development and sensitivity to initial conditions, *Environ. Model. Softw.*, 24, 611–626, doi:10.1016/j.envsoft.2008.10.001.
- Cunningham, A. B., W. G. Characklis, F. Abedeen, and D. Crawford (1991), Influence of biofilm accumulation on porous media hydrodynamics, *Environ. Sci. Technol.*, 25, 1305–1310, doi:10.1021/es00019a013.
- Davey, M. E., N. C. Caiazza, and G. A. O’Toole (2003), Rhamnolipid surfactant production affects biofilm architecture in *Pseudomonas aeruginosa* PAO1, *J. Bacteriol.*, 185(3), 1027–1036, doi:10.1128/JB.185.3.1027-1036.2003.
- Davis, C. A., E. A. Atekwana, E. A. Atekwana, L. D. Slater, S. Rossbach, and M. R. Mormile (2006), Microbial growth and biofilm formation in geologic media is detected with complex conductivity measurements, *Geophys. Res. Lett.*, 33, L18403, doi:10.1029/2006GL027312.
- DeJong, J. T., M. B. Fritzes, and K. Nusslein (2006), Microbially induced cementation to control sand response to undrained shear, *J. Geotech. Geoenviron. Eng.*, 132(11), 1381–1392, doi:10.1061/(ASCE)1090-0241(2006)132:11(1381).
- DeJong, J. T., B. M. Mortensen, B. C. Martinez, and D. C. Nelson (2010), Bio-mediated soil improvement, *Ecol. Eng.*, 36, doi:10.1016/j.ecoleng.2008.12.029.
- Dunsmore, B. C., C. J. Bass, and H. M. Lappin-Scott (2004), A novel approach to investigate biofilm accumulation and bacterial transport in porous matrices, *Environ. Microbiol.*, 6(2), 183–187, doi:10.1046/j.1462-2920.2003.00546.x.
- Klapper, I., C. J. Rupp, R. Cargo, B. Purvedorj, and P. Stoodley (2002), Viscoelastic fluid description of bacterial biofilm material properties, *Biotechnol. Bioeng.*, 80(3), 289–296, doi:10.1002/bit.10376.

- Klausen, M., A. Heydorn, P. Ragas, L. Lambertsen, A. Aaes-Jørgensen, S. Molin, and T. Tolker-Nielsen (2003), Biofilm formation by *Pseudomonas aeruginosa* wild type, flagella and type IV pili mutants, *Mol. Microbiol.*, *48*(6), 1511–1524, doi:10.1046/j.1365-2958.2003.03525.x.
- Lesmes, D. P., and K. M. Frye (2001), Influence of pore fluid chemistry on the complex conductivity and induced polarization responses of Berea sandstone, *J. Geophys. Res.*, *106*, 4079–4090, doi:10.1029/2000JB900392.
- Li, X., and L. J. Pyrak-Nolte (1998), Acoustic monitoring of water–sediment interaction, *Geophys. Res. Lett.*, *25*(20), 3899–3902, doi:10.1029/1998GL900028.
- Li, X., L. R. Zhong, and L. J. Pyrak-Nolte (2001), Physics of partially saturated porous media: Residual saturation and seismic-wave propagation, *Annu. Rev. Earth Planet. Sci.*, *29*, 419–460, doi:10.1146/annurev.earth.29.1.419.
- Liu, C. H., and S. R. Nagel (1992), Sound in sand, *Phys. Rev. Lett.*, *68*(15), 2301–2304, doi:10.1103/PhysRevLett.68.2301.
- Marshall, K. C. (1992), Biofilms: An overview of bacterial adhesion, activity, and control at surfaces, *ASM News*, *58*(4), 202–207.
- Mavko, G., and D. Jizba (1991), Estimating grain-scale fluid effects on velocity dispersion in rocks, *Geophysics*, *56*, 1940–1949, doi:10.1190/1.1443005.
- Nihei, K. T. (1992), Micromechanics of seismic wave propagation in granular rocks, Ph.D. thesis, 167 pp., Univ. of Calif., Berkeley.
- Nolte, D. D., L. J. Pyrak-Nolte, J. Beachy, and C. Ziegler (2000), Transition from the displacement discontinuity limit to the resonant scattering regime for fracture interface waves, *Int. J. Rock Mech. Min. Sci.*, *37*(1–2), 219–230, doi:10.1016/S1365-1609(99)00102-1.
- Palmer, I. D., and M. L. Traviolia (1980), Attenuation by squirt flow in undersaturated gas sands, *Geophysics*, *45*, 1780–1792, doi:10.1190/1.1441065.
- Pamp, S. J., and T. Tolker-Nielsen (2007), Multiple roles of biosurfactants in structural biofilm development by *Pseudomonas aeruginosa*, *J. Bacteriol.*, *189*(6), 2531–2539, doi:10.1128/JB.01515-06.
- Pyrak-Nolte, L. J., B. L. Mullenbach, X. Li, D. D. Nolte, and A. S. Grader (1999), Detecting sub-wavelength layers and interfaces in synthetic sediments using seismic wave transmission, *Geophys. Res. Lett.*, *26*, 127–130, doi:10.1029/1998GL900237.
- Slater, L., and D. P. Lesmes (2002), IP interpretation in environmental investigations, *Geophysics*, *67*, 77–88, doi:10.1190/1.1451353.
- Slater, L., F. D. Day-Lewis, D. Ntarlagiannis, M. O'Brien, and N. Yee (2009), Geoelectrical measurement and modeling of biogeochemical breakthrough behavior during microbial activity, *Geophys. Res. Lett.*, *36*, L14402, doi:10.1029/2009GL038695.
- Stoodley, P., Z. Lewandowski, J. D. Boyle, and H. M. Lappin-Scott (1999), Structural deformation of bacterial biofilms caused by short-term fluctuations in fluid shear: An in situ investigation of biofilm rheology, *Biotechnol. Bioeng.*, *65*(1), 83–92, doi:10.1002/(SICI)1097-0290(19991005)65:1<83::AID-BIT10>3.0.CO;2-B.
- Williams, K. H. (2002), Monitoring microbe-induced physical property changes using high-frequency acoustic waveform data: Toward the development of a microbial megascope, M.S. thesis, Univ. of Calif., Berkeley.
- Williams, K. H., D. Ntarlagiannis, L. D. Slater, A. Dohnalkova, S. S. Hubbard, and J. F. Banfield (2005), Geophysical imaging of stimulated microbial biomineralization, *Environ. Sci. Technol.*, *39*(19), 7592–7600, doi:10.1021/es0504035.
- Yerly, J., Y. Hu, and R. J. Martinuzzi (2008), Biofilm structure differentiation based on multi-resolution analysis, *Biofouling*, *24*(5), 323–337, doi:10.1080/08927010802209892.
- Zhan, X. M., M. Rodgers, and E. O'Reilly (2006), Biofilm growth and characteristics in an alternating pumped sequencing batch biofilm reactor (APSBRR), *Water Res.*, *40*, 817–825, doi:10.1016/j.watres.2005.12.003.

E. A. Atekwana, Boone Pickens School of Geology, Oklahoma State University, Stillwater, OK 74078, USA. (estella.atekwana@okstate.edu)
 C. A. Davis, Department of Geological Sciences and Engineering, Missouri University of Science and Technology, Rolla, MO 65409, USA.
 M. E. Haugen and L. J. Pyrak-Nolte, Department of Physics, Purdue University, West Lafayette, IN 47907, USA.
 D. D. Werkema Jr., U.S. Environmental Protection Agency, Las Vegas, NV 89119, USA.